



HAL
open science

The Influence of Si on the High-Temperature Oxidation of Near-alpha Titanium Alloys

Virgil Optasanu, Benjamin Vincent, Pascal Berger, María del Carmen Marco de Lucas, Tony Montesin, Luc Lavis

► **To cite this version:**

Virgil Optasanu, Benjamin Vincent, Pascal Berger, María del Carmen Marco de Lucas, Tony Montesin, et al.. The Influence of Si on the High-Temperature Oxidation of Near-alpha Titanium Alloys. High Temperature Corrosion of Materials, 2024, 101 (6), pp.1355 - 1367. 10.1007/s11085-024-10310-6 . hal-04768307

HAL Id: hal-04768307

<https://minesparis-psl.hal.science/hal-04768307v1>

Submitted on 5 Nov 2024

HAL is a multi-disciplinary open access archive for the deposit and dissemination of scientific research documents, whether they are published or not. The documents may come from teaching and research institutions in France or abroad, or from public or private research centers.

L'archive ouverte pluridisciplinaire **HAL**, est destinée au dépôt et à la diffusion de documents scientifiques de niveau recherche, publiés ou non, émanant des établissements d'enseignement et de recherche français ou étrangers, des laboratoires publics ou privés.



The Influence of Si on the High-Temperature Oxidation of Near-alpha Titanium Alloys

Virgil Optasanu¹ · Benjamin Vincent¹ · Pascal Berger² ·
María del Carmen Marco de Lucas¹ · Tony Montesin¹ · Luc Lavissee¹

Received: 6 September 2024 / Revised: 6 September 2024 / Accepted: 11 September 2024 /
Published online: 23 September 2024

© The Author(s), under exclusive licence to Springer Science+Business Media, LLC, part of Springer Nature 2024

Abstract

The addition of Si is known to improve the oxidation resistance of pure titanium and titanium alloys. However, most past studies concern the influence of relatively large Si contents (0.35–8 wt%), which is often incompatible with a good ductility because of the presence of Ti_5Si_3 precipitates. This study focuses on the influence of the Si content on the high-temperature resistance of near-alpha alloys from the family of Ti6244 alloy (6% Al, 2% Sn, 4% Zr 4% Mo–wt%) with small proportions of Si. The silicon addition was found to improve the high-temperature oxidation resistance of near-alpha Ti–Al–Sn–Zr–Mo family alloys by decreasing the oxidation rate and the oxide scale thickness, as well by producing a denser oxide scale. Rutile and alumina were detected within the oxide scale by XRD and Raman spectrometry. The presence of Si is associated with the presence of larger quantities of N at the oxide/metal interface.

✉ Virgil Optasanu
virgil.optasanu@u-bourgogne.fr

Benjamin Vincent
benjamin.vincent@iut-dijon.u-bourgogne.fr

Pascal Berger
pascal.berger@cea.fr

María del Carmen Marco de Lucas
carmen.marco-de-lucas@u-bourgogne.fr

Tony Montesin
tony.montesin@u-bourgogne.fr

Luc Lavissee
luc.lavissee@u-bourgogne.fr

¹ ICB UMR 6303 CNRS, Université de Bourgogne, 9 av. Alain Savary, 21078 Dijon Cedex, France

² CEA, CNRS, NIMBE, Université Paris-Saclay, 91191 Gif-sur-Yvette, France

Keywords Near-alpha titanium alloys · Silicon · High-temperature oxidation

Introduction

The use of titanium alloys in aeronautic industries is continuously growing thanks to the interesting mechanical and chemical properties as the good specific strength, good oxidation resistance up to 550 °C for pure titanium and about 600 °C for titanium alloys. The French ANR Project ALTITUDE (2019-2023-IJL Université de Lorraine, ICB Université de Bourgogne, TIMET France, SAFRAN and ONERA) has the general objective to design a new alloy able to reach 650 °C in service, to guarantee improved mechanical properties and high-temperature oxidation resistance. One of the ways to improve the high-temperature oxidation resistance is to finely tune the contents of the alloying elements.

Silicon is known as improving the oxidation resistance of pure titanium [1–5] and titanium alloys (TA6V) [6]. However, most of the studies in the literature investigate the influence of quite large Si contents (0.35–8 wt%). Generally, such high Si contents are incompatible with good ductility because of the presence of brittle Ti_5Si_3 precipitates. At high temperatures, these precipitates effectively hinder dislocations movement which improves the creep behavior of titanium alloys.

Chaze and Coddet [1] studied the oxidation of Ti-Si alloys with 0.25, 0.5 and 1 wt% of Si at temperatures between 550 °C and 750 °C for exposures up to 500 h in air and several thousands of hours in air. They reported that the increasing Si content promotes the oxidation resistance of the alloys by decreasing the mass gain, the oxide thickness as well the oxygen diffusion zone into the metal beneath the oxide layer. Vojtek et al. [2] have studied higher silicon contents (2 and 8 wt%) and mentioned that there are no significant differences in terms of mass gain between the two silicon contents. For 8% wt of silicon, the oxide present dispersed SiO_2 particles, which seems to delay the recrystallization of the rutile and then the stratification of the oxide scale, leading to denser oxide layers. Habazaki et al. [7] have studied the anodization of Ti-6%Si alloy and have reported that the silicon is not evenly distributed into the oxide scale but rather close to the interface oxide/metal and conclude that the Si atoms are relatively immobile into the oxide. Valenza et al. [5] have observed finely dispersed SiO_2 particles within the rutile layer of oxidized Ti-XT (Ti-0.45%Si wt%).

Several studies have pointed out the role of the nitrogen in the oxidation of the titanium and titanium alloys in air. Chaze and Coddet [8] have shown that titanium and some binary alloys oxidize slower in air than in pure oxygen. Recent works have reported the quantities of nitrogen involved into the oxidation in air for pure titanium [9] and shown the strong correlation between the nitrogen quantity involved and the total mass gain for near-alpha titanium alloys [10].

We focus in this study on the influence of the Si content on the high-temperature oxidation resistance of near-alpha alloy Ti6244 (6% Al, 2% Sn, 4% Zr 4% Mo–wt%) and two of its variants containing small proportions of 0.11 wt% and 0.22 wt% of Si.

Table 1 Composition of the alloys

Alloy	Al wt%	Sn wt%	Zr wt%	Mo wt%	Si wt%
Ti6244	5.8	2.1	4.1	3.8	0
Ti6244-0.11%Si	5.6	2	4	3.7	0.11
Ti6244-0.22%Si	5.7	2.1	4.1	3.7	0.22

Table 2 Oxidation results for Ti6244, Ti6244-0.11%Si, and Ti6244-0.22%Si alloys

Alloy	Oxidation time (h)	Temperature (°C)	k_p ($\times 10^{-14}$ g ² /cm ⁴ ·s)	Ea(kJ/mol)
Ti6244	10000	560	2.5 ± 0.1	208 ± 6
	5000	600	7.6 ± 0.6	
	3000	650	47 ± 3	
	50	700	83.5 ± 0.1	
Ti6244-0.11%Si	10000	560	1.9 ± 0.1	190 ± 3
	5000	600	6.7 ± 0.5	
	3000	650	27.5 ± 0.4	
	50	700	75.2 ± 0.1	
Ti6244-0.22%Si	10000	560	1.9 ± 0.1	
	5000	600	5.7 ± 0.3	
	3000	650	27.20.9	
	50	700	66.2 ± 0.1	

Experimental Procedures

Three different alloys were manufactured by TIMET (France): Ti6244 (with no Si), Ti6244 with 0.11 wt% of Si (here called Ti6244-0.11%Si) and Ti6244 with 0.22 wt% of Si (here called Ti6244-0.22%Si). The alloys were produced by TIMET (France) in the form of small ingots synthesized by vacuum arc remelting. The measured compositions of these alloys were made by inductively coupled plasma (ICP) and verified by X-Ray fluorescence. The compositions are given in Table 1. The main role of the alloying elements is: the Al hardens and strengthens the α -Ti phase, the Mo enhances the mechanical strength, the Zr reduces the brittleness, the Sn enhances the creep resistance and strengthens the α -Ti phase, while the Si increases the resistance to creep.

The ingots are beta-forged, rolled and solution treated in beta-phase at 1015 °C, followed by air cooling to room temperature to obtain a lamellar microstructure, then aged for 2 h at 650 °C and subsequently air-cooled. Cylindrical rods about 12 mm diameter are lathe machined. Two-mm-thick samples are wheel-cut. The samples are polished up to P600 grit, then ultrasonic cleaned in ethanol, dried, measured and weighted and then oxidized in muffle furnace under atmospheric air or in TGA under dry air. The conditions of oxidation, with durations and temperatures are presented in Table 2. Investigations by scanning

electron microscopy (SEM) in BSE mode, X-ray diffraction (XRD), Raman spectroscopy, microhardness, secondary ion mass spectrometry (SIMS) and nuclear reaction analysis are made. The SIMS measurements are made on a NanoTOF II apparatus (ULVAC-PHI). The TOF analyses are done using Bi_3^{2+} primary ions in $40 \times 40 \mu\text{m}^2$ area at 30 keV. Cs^+ ions in $200 \times 200 \mu\text{m}^2$ (at 2 keV and 2nA) are used before analysis for sputtering purposes. The microhardness $\text{HV}_{0.02}$ is made with a Vickers penetrator using 20 g of load for 10 s at maximum load. Nitrogen quantifications are made by nuclear reaction analysis which is produced by high-energy deuterium ions (here 1.9 MeV) beam techniques at LEEL lab from CNRS/CEA Saclay, France. The nuclear reaction used in this work is $^{14}\text{N}(d, \alpha)^{12}\text{C}$. The investigated zone is $200 \times 200 \mu\text{m}^2$. Details about this technique can be found in some of our previous works [9–11].

Raman spectroscopy was made using a Renishaw Invia device with a laser excitation source at 532 nm and a microscope objective at $\times 100$ magnification. The Raman fingerprint of TiO_2 in both rutile and anatase phases is detected in the $100\text{--}1000 \text{ cm}^{-1}$ range. The laser excitation at 532 nm can also give rise to the strong photoluminescence of Cr^{3+} ions inserted in octahedral sites in the alpha-alumina lattice. The spectrum of this photoluminescence can be easily identified by the narrow $R1$, $R2$ lines at 691.9 nm and 693.4 nm, respectively. This spectral range corresponds to a Raman shift around 4350 cm^{-1} in the spectra obtained with a laser at 532 nm, which is quite far from the fingerprint of TiO_2 . The cross section of samples oxidized for 3000 h was analyzed in both spectral ranges. Line profiles through the oxidation layer and maps displaying the integrated intensity over the baseline were obtained for the Raman signals of rutile and anatase phases of TiO_2 , and the photoluminescence of $\text{A}_2\text{O}_3: \text{Cr}^{3+}$. The integrated intensity of these three signals was normalized to easily compare the profiles for each sample, except for the anatase phase in Ti6244 due to its extremely low signal.

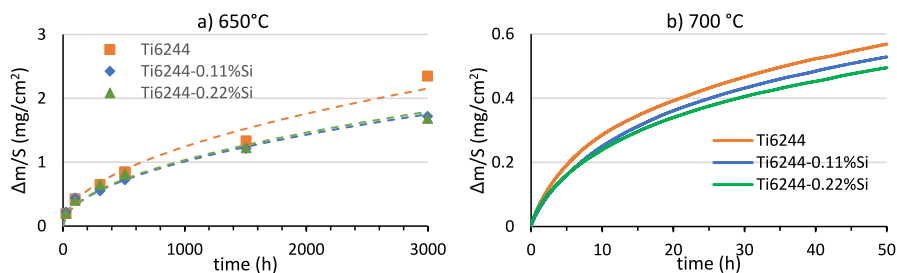


Fig. 1 Mass gain per unit surface: **a** during long oxidation tests at 650°C in muffle furnace (the dashed lines are guides for the eyes) and **b** during short oxidation in TGA at 700°C in dry synthetic air

Results and Discussion

Long-duration oxidation tests under laboratory air are made in muffle furnace at various temperatures: 560 °C, 600 °C and 650 °C for 10,000 h, 5000 h and 3000 h, respectively. The mass gain graphic is presented in Fig. 1 (a) for long exposure at 650 °C, with each point representing an individual sample. As reported, the mass gain during the exposure at 650 °C up to 3000 h shows parabolic kinetics for the alloys containing Si. At the opposite, mass gain of the alloys without Si seems to have a parabolic behavior up to 1500 h but suggests a breakaway before 3000 h of exposure. The mass gain after 3000 h at 650 °C is 2.35 mg/cm² for Ti6244 and about 1.7 mg/cm² for Ti6244-0.11%Si and Ti6244-0.22%Si. This confirms the beneficial effect of the presence of silicon on minimization of the oxidation rate. However, the difference in behavior is not very different between the two alloys containing silicon, which suggests that, for exposures up to 3000 h at 650 °C, small amounts of silicon are sufficient to assure a protective oxide layer. The calculated parabolic constants k_p are listed in Table 2, with standard errors. For the 6244 sample, the parabolic constant k_p was calculated using data up to 1500 h (before breakaway).

To investigate the influence of the silicon on the oxidation kinetics at higher temperatures, TGA oxidation experiments were performed. To assure reasonable oxidation times, compatible with TGA analysis, the alloys were exposed at 700 °C (heating rate 50 °C/min) for 50 h under dry synthetic air flow of 40 ml/min. The kinetics presented in Fig. 1b show parabolic behavior. One can remark that the increasing silicon content decreases the mass gain, and that up to 50 h no breakaway is experienced. For the TGA analysis at 700 °C, the oxidation parabolic constant k_p presented in Table 2 was calculated using a complete parabolic function [12] by excluding the first 16 h of oxidation to avoid the transitory period. Thus, using all the data from 560 to 650 °C (to respect the same oxidation atmosphere, i.e., atmospheric air) one can calculate the activation energies (see Table 2). The standard error of the activation energy calculated using the tunnel technique is given. One can remark that the presence of silicon lowers the activation energy but that there is no difference between both alloys containing Si. These activation energies are compatible with those reported in literature for titanium and similar near-alpha titanium alloys [1, 8].

The first row of Fig. 2 shows the oxide scale morphology for the three alloys studied here after 3000 h of exposure at 650 °C in air. On the metal side, both titanium phases alpha (gray) and beta (white) can be observed. The structure is a typical Widmanstätten obtained by the thermal treatment after forging. The alpha phase is enriched in Al while the beta one is enriched in Mo. One must mention that oxide scale thickness is not constant along the sample surface, which makes difficult to give a precise thickness of the layer. The measured oxide scale thicknesses made using several micrographs for Ti6244, Ti6244-0.11%Si, and Ti6244-0.22%Si are $4.7 \pm 0.5 \mu\text{m}$, $3.4 \pm 0.3 \mu\text{m}$, and $2.8 \pm 0.5 \mu\text{m}$, respectively. The oxide is layered and seems denser on the alloys containing Si. Other authors [1, 5] have shown that the rutile presents a fine dispersion of SiO₂ which is supposed to modify the stress relaxation process and then produce denser oxide layers.

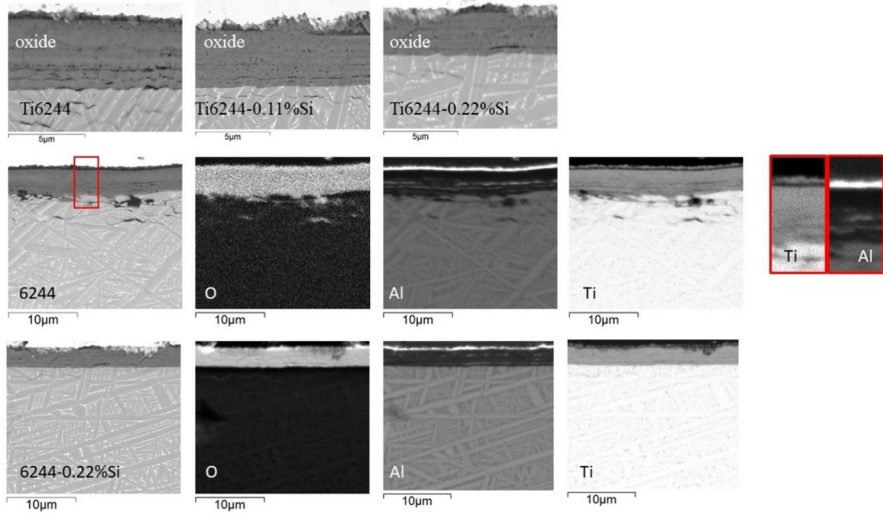


Fig. 2 SEM images of cross section of oxidized alloys at 650 °C in air for 3000 h with EDS mappings and red insets with zoomed Ti and Al mapping for Ti6244 alloy

Analyzing the EDS maps of Ti6244 and Ti6244-0.22%Si (Fig. 2), the predominant component of the oxide scale (a few μm thick) is primarily titanium oxide. Aluminum oxide is predominantly present in a thin layer approximately 200 nm thick on the outer surface of the oxide, as well as in the cracks visible as light gray strips in the middle of the oxide scale in the EDS map of aluminum. Interestingly, the presence of a very thin layer of titanium, together with oxygen, is observed above the top alumina layer for Ti6244. This very thin layer is visible in the zoomed-in titanium mapping of the red insets shown in Fig. 2 for Ti6244. If present, this layer would be thinner for Ti6244-0.22%Si. This kind of $\text{TiO}_2/\text{Al}_2\text{O}_3/\text{TiO}_2$ layering was also observed by Ke et al. on Ti-5Al after oxidation at 600 °C and 800 °C for 96h [13]. The oxide layer of the Ti6244 sample seems to be more stratified, with intermediary alumina strips for than for the other two alloys. The acceleration of the kinetic observed in Fig. 1.a for this alloy can probably be related to this stratification. The low Si content within the alloys, as well as the fact that the cross section of the samples was polished using Si-containing particles (SiC paper and colloidal silica for the super-finishing step), makes in this case the detection and the localization of the Si after oxidation hazardous and must be deeper investigated. Moreover, the Si is present in the metal in the form of nanometric Ti_5Si_3 precipitates located at the α/β phases interface as well as at grain boundaries as shown by several studies [14, 15]. Chaze and Coddet [1] detected SiO_2 particles in the oxide scale by MET in TiSi alloys. Valenza et al. [5] have detected a fine dispersion of SiO_2 within the rutile for Ti-4.5%Si after oxidation at 800 °C.

The Ti6244 and Ti6244-0.22%Si oxidized at 650 °C for 3000 h were investigated by XRD in theta–theta mode and in low-angle incidence mode at a grazing angle of 4°. The XRD patterns recorded in theta–theta mode presented in Fig. 3 reveal the

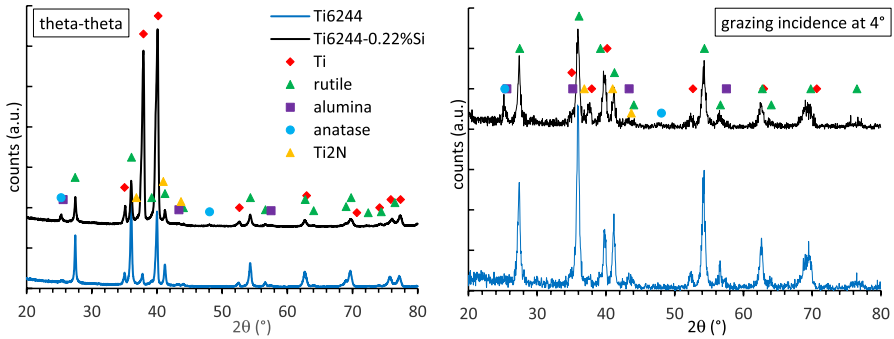


Fig. 3 XRD patterns for Ti6244 and 6244-0.22%Si after oxidation for 3000 h at 650 °C in theta–theta mode (left) and grazing incidence at 4° (right)

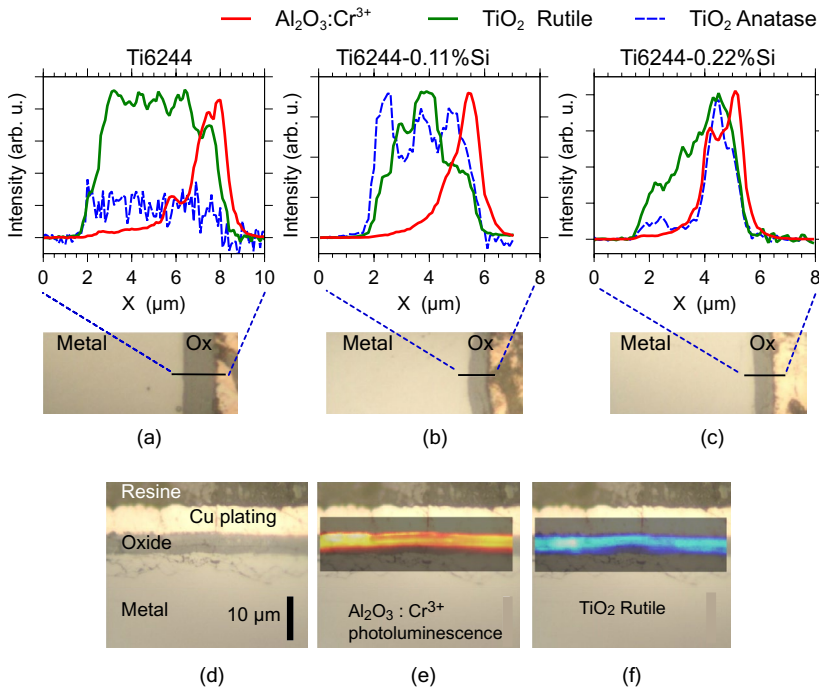


Fig. 4 **a, b, c** Evolution of the integrated intensity of the Raman signals of the rutile and anatase phases, as well as the intensity of alpha-Al₂O₃: Cr³⁺ photoluminescence, along the cross section of the oxide scale for Ti6244, Ti6244-0.11%Si, and Ti6244-0.22%Si alloys oxidized for 3000 h at 650 °C. **d** Cross-sectional optical micrography of Ti6244 sample oxidized for 3000 h at 650 °C, **e** mapping of the alumina photoluminescence and **f** mapping of rutile Raman signal in the selected area of the cross section

presence of rutile, slightly distorted alpha titanium and suggest small amounts of anatase and alumina. Also, the presence of a small quantity of Ti₂N is suggested, as already mentioned on Ti6242S alloy by Abdallah et al. [17]. The grazing incidence

mode shows mainly the rutile and confirm the presence of Ti_2N , especially in the Ti6244-0.22%Si alloy.

Cross sections of the three alloys oxidized at 650 °C for 3000 h were also analyzed by micro-Raman spectroscopy (Fig. 4), which confirmed the dominant presence of rutile in the oxide scale. The anatase phase was almost absent in the oxide scale for Ti6244, but its proportion increased with Si content. In a very high spectral range, very intense photoluminescence of Cr^{3+} ions was observed in alpha-alumina. Figure 4a, b, c shows the evolution of the integrated intensity of the Raman signals of the rutile and anatase phases, as well as the intensity of alpha- Al_2O_3 : Cr^{3+} photoluminescence, along the cross section of the oxide scale. It is worth recalling the very high sensitivity of photoluminescence for the detection of alpha- Al_2O_3 : Cr^{3+} . It was found that alumina is mainly present in the outer part of the scale, in agreement with the EDS maps, but is also present throughout the thickness of the oxide. For Ti6244, EDS maps showed a very thin layer of titanium oxide above the top alumina layer, but Raman spectra do not show the presence of rutile at the extreme surface, maybe due to a poor crystallization of this titanium oxide thin layer. Figure 4e, f shows Raman maps of the distribution of rutile and alumina throughout the cross section of Ti6244 alloy oxidized for 3000 h at 650 °C. They agree with the profiles shown in Fig. 4a, and they show the presence of alumina in the cracks formed in the oxide scale.

Figure 5 shows the microhardness profiles, which reveal the extent of the oxygen diffusion zone, since the oxygen dissolved into the hexagonal lattice of the alpha titanium hardens the metal. As observed, there are no significant differences between the three alloys in terms of oxygen depth of penetration into the core of material. The same conclusion was drawn by Valenza et al [5] on Ti-XT (Ti-0.45%Si) alloy compared to pure Ti during oxidation in air at 800 °C. The oxygen diffusion length at 650 °C after 3000 h is about 200 μm while at 600 °C this is about 100 μm . The silicon seems to reduce the hardness of the metal close to the interface with the oxide at 650 °C. One of the reasons of this behavior can be the modification of the solubility of the oxygen into the metal, but this hypothesis must be confirmed by further analyses. Valenza et al. [5] found by tomography that there is no difference

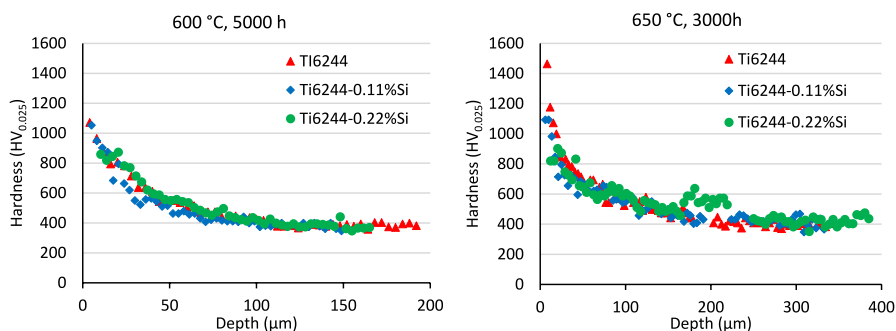


Fig. 5 Microhardness profiles for Ti6244, Ti6244-0.11%Si, and Ti6244-0.22%Si after oxidation for 5000 h at 600 °C and 3000 h at 650 °C. The standard error for hardness measurements is 19 HV

in solubility between Ti-4.5%Si and pure Ti after oxidation at 800 °C in oxygen. They also evidenced a layer of about 10 nm of Ti₅Si₃ at the interface oxide/metal.

A rapid calculation based on the density of the rutile (4.25 g/cm³) shows that 1 μm thick of dense TiO₂ rutile represents 0.169 mg/cm² of oxygen. This indicates that, in the hypothesis of a dense rutile scale, after exposure at 650 °C for 3000 h, the oxygen contained into the oxide layer is about 0.8, 0.6 and 0.44 mg/cm² for Ti6244, Ti6244-0.11%Si and Ti6244-0.22%Si, respectively. The difference between the total mass gain and the oxygen mass contained into the oxide scale is diffusing into the metal (in the hypothesis that the nitrogen quantity is negligible):

$$\left(\frac{\Delta m}{S}\right)_{\text{diff}} = \left(\frac{\Delta m}{S}\right)_{\text{total}} - \left(\frac{\Delta m}{S}\right)_{\text{oxide}}$$

Here, the diffused oxygen quantities become 1.5, 1.1 and 1.26 mg/cm² in Ti6244, Ti6244-0.11%Si and Ti6244-0.22%Si, respectively.

The quantity of oxygen contained into the diffusion zone can be calculated with [16]:

$$\left(\frac{\Delta m}{S}\right)_{\text{diff}} = \rho_{\text{alloy}} \frac{M_{\text{O}}}{M_{\text{alloy}}} \int_0^{\infty} (c(x) - c_0) dx \tag{1}$$

with M_{O} and M_{alloy} the molar mass of oxygen and alloy, ρ_{alloy} the density of the alloy, $c(x)$ the atomic oxygen concentration into the alloy and c_0 the atomic oxygen concentration at the core of the metal. By taking the $c_0 = 0$ and assuming that the concentration follows a classical conjugated error function $c(x) = c_s \operatorname{erfc}\left(\frac{x}{2\sqrt{Dt}}\right)$ then:

$$\left(\frac{\Delta m}{S}\right)_{\text{diff}} = \rho_{\text{alloy}} \frac{M_{\text{O}}}{M_{\text{alloy}}} \int_0^{\infty} c_s \operatorname{erfc}\left(\frac{x}{2\sqrt{Dt}}\right) dx \tag{2}$$

Knowing that

$$\int_0^{\infty} \operatorname{erfc}(x) dx = \frac{1}{\sqrt{\pi}} \tag{3}$$

It follows:

$$\int_0^{\infty} c_s \operatorname{erfc}\left(\frac{x}{2\sqrt{Dt}}\right) dx = \frac{2}{\sqrt{\pi}} c_s \sqrt{Dt} \tag{4}$$

Then:

$$\left(\frac{\Delta m}{S}\right)_{\text{diff}} = \rho_{\text{alloy}} \frac{M_{\text{O}}}{M_{\text{alloy}}} \frac{2}{\sqrt{\pi}} c_s \sqrt{Dt} \tag{5}$$

The diffusion length depends on the diffusion coefficient and the exposure time as [3]:

$$L_{\text{diff}} = 4\sqrt{Dt} \quad (6)$$

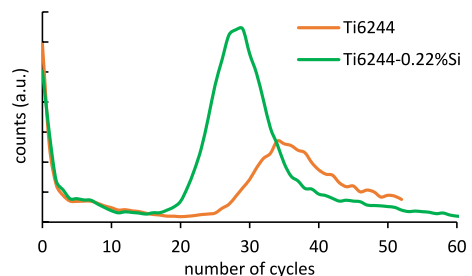
which gives:

$$\left(\frac{\Delta m}{S}\right)_{\text{diff}} = \rho_{\text{alloy}} \frac{M_{\text{O}}}{M_{\text{alloy}}} \frac{c_{\text{S}}}{2\sqrt{\pi}} L_{\text{diff}} \quad (7)$$

This equation allows us to estimate the c_{S} from the mass balance (Eq. 1). Based on the hardness profile after 3000 h at 650 °C (Fig. 3), the length of diffusion can be estimated at ~210 μm, which corresponds to an effective diffusion coefficient of $\sim 2.55 \times 10^{-16} \text{m}^2/\text{s}$, calculated from $L_{\text{diff}} = 4\sqrt{D_{\text{eff}} \times t}$ [3]. From eq. (7), one can estimate the maximum concentration of the oxygen into the alloys as: 17.7 at%, 13 at% and 14.8 at% for Ti6244, Ti6244-0.11%Si and Ti6244-0.22%Si, respectively. These results agree with the hardness profile after exposure at 650°C for 3000 h (see Fig. 3.), where one can remark higher hardening for Ti6244 close to the oxide/metal interface compared with the other two alloys. We must remark that the microhardness profile does not perfectly fit an error function, and because the oxide scale is not 100% dense, the previous concentrations must be considered only qualitatively. Deeper investigations are needed to precisely measure the oxygen concentration profiles.

Our previous investigations [10] have shown that the mass gain of near-alpha titanium alloys is strictly correlated with the nitrogen quantity involved into the oxidation process. Here, the beginning of the oxidation at 650 °C was investigated by SIMS to highlight the nitrogen insertion at the first moments of oxidation. Figure 6 shows the nitrogen profile for Ti6244 and Ti6244-0.22%Si after 25 h of exposure at 650 °C in atmospheric air. One can clearly see that, comparatively, the nitrogen quantity is much higher in the sample containing 0.22% of silicon than in the sample without that element. Several works in the literature have shown that the nitrogen is located at the oxide/metal interface [9–11, 17, 18]. Here one can see that the nitrogen peak of Ti6244-0.22%Si is the most intense and is located closer to the sample surface than for Ti6244, which agrees with a smaller thickness of the oxide scale for Ti6244-0.22%Si as shown in Fig. 2. Other nitrides or oxynitrides [17] can be present in the samples, but the angular resolution of the laboratory XRD technique used here is not sufficient to confirm them.

Fig. 6 Nitrogen profiles obtained by SIMS in erosion mode after 25 h at 650°C. The number of cycles is proportional to the depth from the outer oxide surface



The nuclear reaction analysis was used to quantify and localize the nitrogen. It allows to quantify and locate the nitrogen in the depth of the material. Indeed, the energy of the alpha particles produced by one high-energy deuteron when encounters one ^{14}N isotope can allow to calculate the depth at which the reaction occurs. The number of reactions recorded is proportional to the nitrogen concentration and to the probability of the nuclear reaction to occur (effective cross section of the reaction). Thus, quantitative nitrogen profiles can be deduced, as shown in Fig. 7. By integration of the signal, one can calculate the total nitrogen quantity in terms of mass gain, which in this case is $52 \mu\text{g}/\text{cm}^2$, $77 \mu\text{g}/\text{cm}^2$ and $83 \mu\text{g}/\text{cm}^2$ for Ti6244, Ti6244-0.11%Si and Ti6244-0.22%Si, respectively. However, one must precise that given the fact that the Al nuclear reactions give small signals in regions close to those of $^{14}\text{N}(\text{d},\alpha)^{12}\text{C}$ and also that alumina is present into the whole oxide thickness (as detected by Raman), the nitrogen quantities are probably slightly overestimated within the oxide region. But, as observed in Fig. 7 in the range 0.5–1 μm depth, the signal of a dense and pure alumina (which is always present on the top of the rutile layer of these alloys) is small, which makes us consider that the quantification uncertainties given by the Al interferences are negligible compared to the integrated value. From Fig. 7, one can also remark that the nitrogen is located closer to the surface of the sample for the alloys containing silicon, which is expected, since those samples present a thinner oxide scale, as seen on the SEM images.

As already mentioned in a previous work [10], the oxidation resistance is improved when the nitrogen content is high for quasi-alpha titanium alloys in the family of Ti6242S. Here, the silicon is responsible for both, the oxidation resistance, and the nitrogen mass gain. Thus, one can confirm that the silicon promotes the nitrides formation, as remarked by the XRD analyses. The presence of a bigger quantity of nitrogen can produce a slowdown of the oxidation by two mechanisms: the formation of nitrides that can partially block the oxygen diffusion toward the metal and the occupation of the octahedral sites of the titanium lattice by the nitrogen. Moreover, the presence of nitrides and their location (on the metal side, as shown in [9]) suggests that in the regions with nitrides, the oxidation process follows

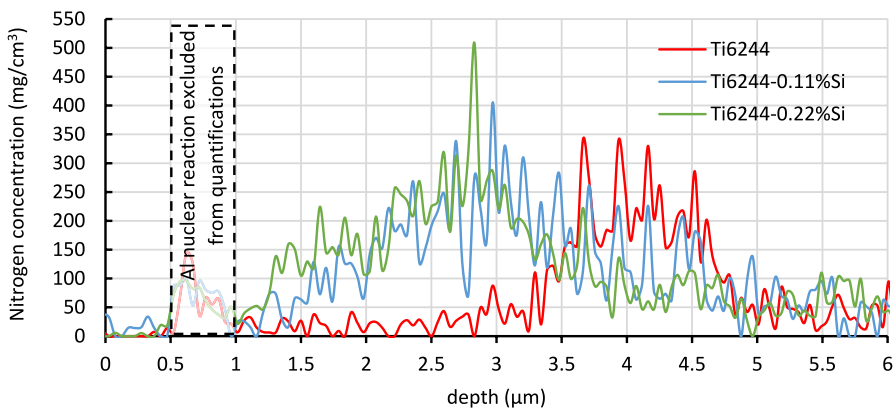


Fig. 7 Nitrogen concentration profile obtained by nuclear reaction analysis

a modified reactional path, which can affect the kinetics. The nitrogen released during the oxidation process diffuses further into the metal on short distances to form other nitrides [9]. Moreover, on the metal side, both nitrogen and oxygen occupy the same octahedral sites of the titanium lattice. As the nitrogen atom is bigger than the oxygen, its diffusion coefficient is about two decades smaller than that of oxygen [19]; thus, by occupying the same sites, it impedes the oxygen flux. Also, the fact that the Ti/Ti₂N reaction has a lower Pilling–Bedworth ratio (1.06) than that of the Ti/TiO₂ rutile reaction (1.765) strongly suggests that these nitrides can play the role of an accommodation layer that lowers the stress. The fact that the Si-containing alloys exhibit denser oxide scales, as seen in Fig. 2, tends to confirm this hypothesis.

Conclusion

This article investigates the oxidation behaviors of three titanium alloys with different contents of silicon as alloying element: the reference Ti6244 alloy (6% Al, 2% Sn, 4% Zr, 4% Mo–wt%), Ti6244–0.11%Si alloy (6% Al, 2% Sn, 4% Zr, 4% Mo, 0.11% Si) and Ti6244–0.22%Si alloy (6% Al, 2% Sn, 4% Zr, 4% Mo, 0.22% Si).

The thermogravimetric analyses and SEM observations show that the presence of silicon slightly decreases the mass gain and reduces the oxide scale thickness but does not have significant influence on the depth of penetration of the oxygen into the material with subsequent hardening. However, at 650°C, the presence of Si seems to reduce the maximum concentration of the oxygen into the metal, as suggested by the microhardness profiles. The microhardness profiles allowed to check the mass balance between the total mass gain, the oxygen contained into the oxide and the oxygen contained into the diffusion zone. The micrographic analysis with subsequent EDS mapping showed the oxide morphology composed of a thin layer of TiO₂, followed by a thin layer of Al₂O₃ and a thick layer of TiO₂. Raman analysis showed that both alumina and rutile are detected in the oxide scale. The nuclear reaction analysis revealed that the Si favors the insertion of larger quantities of N at the interface oxide/metal. It also seems to lower the hardness of the solid solution close to the oxide/metal interface, which suggests lower oxygen concentrations, but does not seem to modify the oxygen diffusion coefficient into the metal, since the length of diffusion is not affected. The Ti₂N formed at the oxide/metal interface, which has lower molar volume than TiO₂, becomes probably an adaptation layer that delays the stratification of the oxide scale by lowering the stress level.

Acknowledgement This work is supported by the EIPHI Graduate School (contract ANR-17-EURE-0002) and the French National Research Agency (ALTITUDE project ANR-18-CE08–0024). Special thanks to Nicolas Geoffroy, Frédéric Herbst and Olivier Heintz for the technical support.

Author Contribution V.O. involved in writing—review & editing, validation, methodology, investigation, formal analysis, data curation, conceptualization. B.V. took part in investigation, formal analysis. P.B. involved in investigation, review & editing, formal analysis, conceptualization. MC.ML. involved in writing—review & editing, validation, methodology, investigation, formal analysis, conceptualization. T.M. took part in project administration. L.L.: involved in review & editing, validation, methodology, investigation, conceptualization.

Funding Agence Nationale de la Recherche, EIPHI Graduate School (contract ANR-17-EURE-0002), EIPHI Graduate School (contract ANR-17-EURE-0002).

Data Availability The raw/processed data required to reproduce these findings cannot be shared at this time as the data also form part of an ongoing study. Some data can be available on request. Please contact the corresponding author.

Declarations

Competing Interests The authors declare no competing interests.

References

1. A. M. Chaze and C. Coddet, *Oxidation of Metals* **27**, 1 (1987).
2. D. Vojtěch, B. Bártoňová, and T. Kubařík, *Materials Science and Engineering* **361**, 50 (2003).
3. B. Vincent, V. Optasanu, F. Herbst, et al., *Oxidation of Metals* **96**, 283 (2021).
4. J.-Y. Xu, Z.-Z. Shi, Z.-B. Zhang, H.-G. Huang, and X.-F. Liu, *Corrosion Science* **166**, 108430 (2020).
5. T. C. Valenza, P. Chao, P. K. Weber, O. K. Neill, and E. A. Marquis, *Corrosion Science* **217**, 111110 (2023).
6. K. Maeda, S. Suzuki, K. Ueda, et al., *Journal of Alloys and Compounds* **776**, 519 (2019).
7. H. Habazaki, K. Shimizu, S. Nagata, P. Skeldon, G. E. Thompson, and G. C. Wood, *Corrosion Science* **44**, 1047 (2002).
8. A. M. Chaze and C. Coddet, *Journal of the Less Common Metals* **124**, 73 (1986).
9. V. Optasanu, P. Berger, M. C. Marco de Lucas, et al., *Corrosion Science* **216**, 111072 (2023).
10. V. Optasanu, P. Berger, B. Vincent, et al., *Corrosion Science* **224**, 111547 (2023).
11. L. Lavisse, P. Berger, A. Kanjer, et al., *Corrosion Science* **197**, 110080 (2022).
12. D. Monceau and B. Pieraggi, *Oxidation of Metals* **50**, 477 (1998).
13. X. Ke, J. Zhang, W. Cai, et al., *Vacuum* **227**, 113468 (2024).
14. B. Fu, H. Wang, C. Zou, and Z. Wei, *Materials Characterization* **99**, 17 (2015).
15. M.-L. Anti, V. Collado Ciprés, J. Mouzon, P. Åkerfeldt, and R. Pederson, *MATEC Web of Conferences* **321**, 04021 (2020).
16. N. Vaché, Y. Cadoret, B. Dod, and D. Monceau, *Corrosion Science* **178**, 109041 (2021).
17. I. Abdallah, C. Dupressoire, L. Laffont, D. Monceau, and A. Vande Put, *Corrosion Science* **153**, 191 (2019).
18. C. Dupressoire, M. Descoins, A. Vande Put, et al., *Acta Materialia* **216**, 117134 (2021).
19. H. Nakajima and M. Koiwa, *ISIJ International* **31**, 757 (1991).

Publisher's Note Springer Nature remains neutral with regard to jurisdictional claims in published maps and institutional affiliations.

Springer Nature or its licensor (e.g. a society or other partner) holds exclusive rights to this article under a publishing agreement with the author(s) or other rightsholder(s); author self-archiving of the accepted manuscript version of this article is solely governed by the terms of such publishing agreement and applicable law.